

pubs.acs.org/cm Article

New Structural Distortions in Osmate Perovskite Na_{1-∞}K_∞OsO₃ Synthesized under High Pressure

Published as part of Chemistry of Materials virtual special issue "C. N. R. Rao at 90".

Jie Chen₄ Alexei A. Belik₄ Kazunari Yamaura₄ and Jianshi Zhou



Cite This: Chem. Mater. 2024. 36. 5587-5595

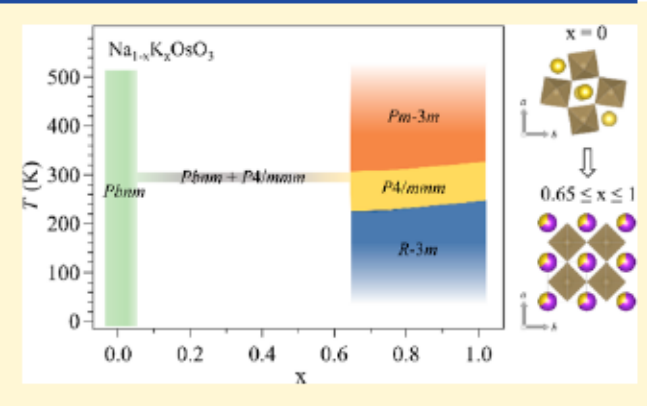


ACCESS I

Metrics & More

Article Recommendations

ABSTRACT: Most ABO₃ oxides crystallize in the perovskite structure. In response to the degree of bonding mismatch of A–O versus B–O in the structure, the perovskite can adopt a total of 15 tilting systems of BO₆ octahedra. Depending on the charge configurations, i.e., $A^{3+}B^{3+}O_3$, $A^{2+}B^{4+}O_3$, and $A^{1+}B^{5+}O_3$, these complex oxides undergo distinct pathways within the tilting systems as the bond length mismatch is changed by either chemical substitution or temperature or pressure. The report of orthorhombic NaOsO₃ and the newly synthesized nearly cubic KOsO₃ lead to an opportunity for studying the structural distortions in $A^{1+}B^{5+}O_3$ which has only been studied in the d⁰ systems of AMO₃ (A = alkaline, M = Nb and Ta). Here, we report the new structural sequence from a cubic perovskite phase to distorted phases as the temperature



decreases in the solid solution of $Na_{1-x}K_xOsO_3$ by synchrotron X-ray powder diffraction; these distorted phases do not belong to the 15 tilting systems. In comparison with the distorted perovskite phases found in the d^0 systems of $A^{1+}B^{5+}O_3$ perovskites, the phase transitions with decreasing temperature found in $Na_{1-x}K_xOsO_3$ are likely caused by the instabilities of their electronic structures.

1. INTRODUCTION

Over the past decade, the intriguing physical properties of the ternary osmate oxides with the A1+Os5+O3 configuration have garnered significant attention. LiOsO3, which adopts a rhombohedral LiNbO3-type structure, undergoes a nonpolar (R3c) to polar (R3c) phase transition at 130 K, while remaining metallic down to the lowest temperature.1 It is commonly referred as a ferroelectric metal or polar metal.2 Due to the smaller Li⁺ occupying the A-site in A^{I+}Os⁵⁺O₃, the geometric tolerance factor $t = (A-O)/(B-O)\sqrt{2}$ of LiOsO₃ (t = 0.86) is too small to adopt a perovskite structure. NaOsO₃ (t = 0.98) synthesized under a pressure of 6 GPa crystallizes in an orthorhombic perovskite structure.3 A metal-insulator transition (MIT) accompanied by a G-type antiferromagnetic ordering was observed in NaOsO₃ at T_{MI} = 410 K. The MIT has been attributed to a Slater transition since there is no abrupt structural change at the transition.4 In the recent years, however, both experimental and theoretical studies suggest that the MIT in NaOsO3 is closely associated with a Mott transition.5,6

Like other perovskite systems with t < 1, it is normal for NaOsO₃ to adopt the orthorhombic *Pbnm* phase for a t = 0.98. The observation that the metal—insulator transition temperature is not sensitive to hydrostatic pressure motivated a study of structural determination under pressure by single-crystal

diffraction with synchrotron X-ray radiation. The *Pbnm* structure remains stable up to 40 GPa, the highest pressure in the study. Significant octahedral site rotations induced under pressure occur in NaOsO₃, which contributes to the majority of compressibility in the oxide, whereas OsO₆ octahedra are less compressible. Increasing the bending angle Os–O–Os, which corresponds to a reduction of the electron bandwidth and therefore compensates the effect of shortening the Os–O bond length under pressure, appears to be responsible for a smaller pressure effect on $T_{\rm MI}$.

The recent successful synthesis of perovskite $KOsO_3$ (t=1) under a high pressure of 14 GPa^8 presents new opportunities to investigate the structural distortions corresponding to the bonding mismatch in the $A^{1+}B^{5+}O_3$ perovskite with occupied d orbitals, where the t factor calculated based on the tabulated ionic radius can be progressively reduced by the chemical substitution in $Na_{1-x}K_xOsO_3$. The perovskite $KOsO_3$ crystal-

Received: February 28, 2024
Revised: May 6, 2024
Accepted: May 6, 2024
Published: May 16, 2024





lizes into a cubic perovskite structure $(Pm\overline{3}m)$ at 500 K and transforms to a tetragonal perovskite structure (P4/mmm) at 320 K, followed by a second transition to a rhombohedral phase $(R\overline{3}m)$ at 230 K. In sharp contrast to other d^0 $A^{1+}B^{5+}O_3$ perovskites where the tilting systems are developed with decreasing t factor, the bond angles Os-O-Os in these structures maintain at 180° through these structural transitions in perovskite KOsO₃. In this article, we report a thorough crystal structural study of $Na_{1-x}K_xOsO_3$ in the phase diagram of the chemical substitution and temperature and compare the new structural distortions with those established for other perovskite compounds.

2. EXPERIMENTAL SECTION

2.1. Sample Synthesis. The polycrystalline solid—solution samples $Na_{1-x}K_xOsO_3$ (x = 0.1, 0.6, 0.65, 0.75, and 1) were synthesized by solid-state reaction under high-pressure and high-temperature conditions. The starting materials KO2 (O2-45.6M, Sigma-Aldrich), Na2O2 (97M, Sigma-Aldrich), and OsO2 (Os-84.0M, Alfa Aesar) were thoroughly mixed in a stoichiometric ratio with 15 mol

excessive KO₂ and Na₂O₂ for reducing the impurities of OsO2 and Os in the final products. The total mass of starting materials for each sample is around 50 mg. The processes of mixing and grinding were conducted in an Ar-filled glovebox; the mixture was sealed in a Pt crucible before taking out from the glovebox. The TEL/EL = 6/12 (TEL = truncated edge length on the cubic anvil and EL = edge length of the pressure-medium octahedron) sample assembly was used in the high-pressure synthesis with a Walker-type-multianvil module (Rockland Research Co.). Under 14 GPa, the samples were heated to a target temperature of 1100 °C and held there for 30 min, followed by a temperature quench to room temperature before releasing the pressure. The temperature quenching was achieved by cutting the power supply, and the sample reached room temperature within 1 min. To mitigate the risk of potential exposure to the highly toxic OsO4, we conducted the preparation of starting materials and opened the sample crucible within an Ar-filled glovebox and a venting hood.

2.2. Powder X-ray Diffraction and Refinement. Each batch of polycrystalline samples was initially checked by powder X-ray diffraction (XRD) with an in-house diffractometer RIGAKU-MiniFlex 600 with Cu K radiation at room temperature. The synchrotron X-ray diffraction (SXRD) measurement was performed on powder samples $Na_{1-x}K_xOsO_3$ (x=0.1, 0.6, 0.65, 0.75, and 1) at room temperature at BL02B2 beamline of SPring-8 with wavelength $\lambda=0.61928$ Å. The temperature-dependent SXRD data of $Na_{1-x}K_xOsO_3$ (x=0.65, 0.75, and 1) was collected from 100 to 400 K at BL02B2 beamline of SPring-8 with wavelength $\lambda=0.61974$ Å. The Rietveld refinement for powder XRD patterns was conducted by RIETAN-FP and VESTA software.

2.3. Measurements of Physical Properties. The magnetic properties of the Na_{1-x}K_xOsO₃ samples were measured in a magnetic property measurement system (MPMS, Quantum Design, Inc.). The polycrystalline samples were encased in copper foil in the measurement. The contribution of the copper capsule was subtracted from the raw data.

The thermoelectric power for the powder sample was measured in a homemade device fitting to the thermal transport option (TTO) in a physical property measurement system (PPMS, Quantum Design, Inc.). The powder sample from grinding the as-grown sample was placed into a 0.7 mm diameter hard plastic die. To verify the reliability of the thermoelectric powder measured on a powder form of a sample, the single-crystal sample NaOsO₃ and the powder sample made by crushing the single-crystal sample were checked, and nearly identical results of the thermoelectric power were obtained.

Differential scanning calorimetry (DSC) measurement was conducted on polycrystalline samples using a Mettler Toledo DSC1 STAR^e system. The samples, 5.57 mg for x = 0.65 and 3.34 mg for x = 0.75, were enclosed within aluminum capsules, respectively. The samples underwent several rounds of DSC measurements to validate its reproducibility.

3. RESULTS

3.1. Structural Characterizations. Figure 1 summarizes the room-temperature results of the phases and their lattice

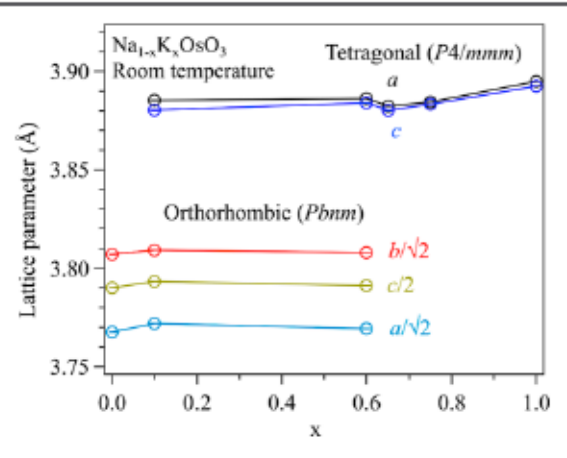


Figure 1. Lattice parameters of $Na_{1-x}K_xOsO_3$ obtained by refining the SXRD patterns collected at room temperature. Error bars are smaller than symbols.

parameters of Na_{1-x}K_xOsO₃ obtained by refining the SXRD patterns. The lattice parameters of the orthorhombic phase for the Na-rich compositions are converted into values in the primary cell. The two-phase coexistence (the tetragonal and the orthorhombic phases) is found in compositions x = 0.1 and 0.6. Negligible changes in lattice parameters in both phases as a function of the nominal concentration x in the range of $0.1 \le x$ ≤ 0.6 indicates that almost all Na stay in the orthorhombic phase and almost all K stay in the tetragonal phase regardless of the nominal composition. The single phase of tetragonal structure T (P4/mmm) is found in the compositions of x > 10.60. All SXRD patterns at room temperature and the refinement results are shown in Figure 2. Results of the phase analysis and lattice parameters are listed in Table 1. We have also refined the patterns for x > 0.6 with another tetragonal structure model (I4/mcm) reported in perovskite oxides such as SrTiO₂ in which there is an antiphase octahedral site titling along the c axis. Despite adopting a larger unit cell in the I4/mcm structure model in comparison with P4/mmm, no significant improvement in R values is obtained. There are no superstructure reflections in the SXRD patterns for x > 0.6 based on the index from the primary cell.

We have chosen the nominal compositions of x = 0.65 and 0.75 with a single phase of the tetragonal structure (at room temperature) for the structural study at different temperatures from 100 to 400 K. The chemical compositions x = 0.573(6)

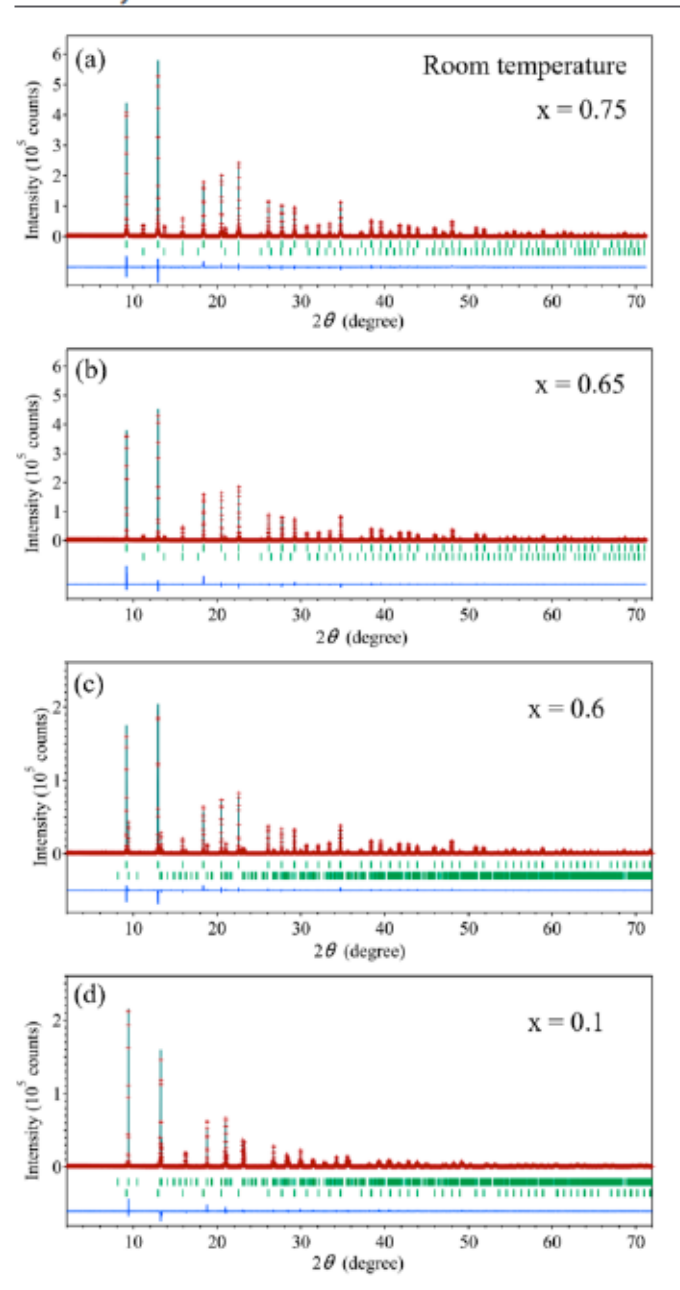


Figure 2. Patterns of SXRD collected at room temperature and the results of Rietveld refinement for $\mathrm{Na_{1-x}}K_x\mathrm{OsO_3}$ (x=0.1,~0.6,~0.65, and 0.75). The crosses and solid lines represent the observed and calculated patterns, respectively, with their differences shown at the bottom. The expected Bragg reflections are marked by ticks for (a–c) P4/mmm structure and (d) Pbmm structure (top); (a,b) $\mathrm{OsO_2}$, (c) Pbmm structure, and (d) P4/mmm structure (bottom).

and 0.77(1) for these two samples were determined based on the SXRD patterns collected at 100 K, which are close to their nominal compositions. It is noted that the occupancy of A-site for the same sample is fixed at the same value during the refinement of SXRD data collected at 120–400 K. The occupancies for the oxygen sites were attempted to refine, and the values of 1.12 and 1.05 are obtained, indicating that these samples are close to oxygen stoichiometric. Thus, the oxygen occupancies were fixed at 1 in the final refinement. We have identified three phases, a cubic phase C $(Pm\bar{3}m)$, T, and a rhombohedral phase R $(R\bar{3}m)$ in the temperature range of 100–400 K. The Na-substitution slightly reduces the lattice parameter in the cubic phase (at 400 K). Typical SXRD patterns and the Rietveld refinement results are present in Figure 3, and the data are listed in Table 2–4.

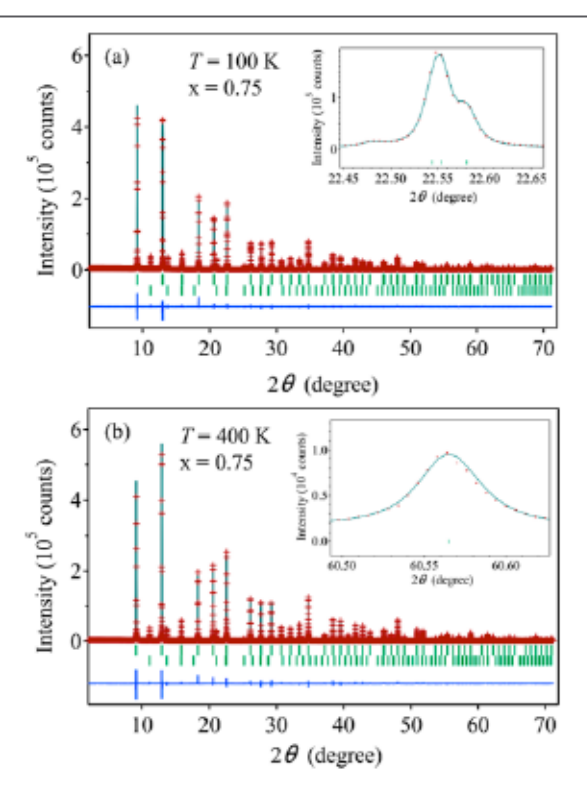


Figure 3. Patterns of SXRD collected at 100 and 400 K and the results of Rietveld refinement for $Na_{1-x}K_xOsO_3$ (x=0.75). The crosses and solid lines represent the observed and calculated patterns, respectively, with their differences shown at the bottom. (a) Expected Bragg reflections are marked by ticks for the $R\overline{3}m$ structure (top) and OsO_2 (bottom). (b) Expected Bragg reflections are marked by ticks for the $Pm\overline{3}m$ structure (top) and OsO_2 (bottom). Similar SXRD profiles (T=100 and 400 K) and the refinement results have been obtained for $Na_{1-x}K_xOsO_3$ (x=0.65).

Table 1. Summary of the Room-Temperature Phases and the Lattice Parameters of Na_{1-x}K_xOsO₃ Obtained by Refining the SXRD Patterns

x	0.1	0.6	0.65	0.75
phases of Na _{1-x} K _x OsO ₃	P4/mmm (2 wt ⊠) Pbnm (98 wt ⋈)	P4/mmm (82 wt ⋈) Pbnm (18 wt ⋈)	P4/mmm	P4/mmm
lattice parameters of tetragonal phase	a = 3.88536(7) Å c = 3.8803(1) Å	a = 3.88621(1) Å c = 3.88397(2) Å	a = 3.88235(2) Å c = 3.88016(4) Å	a = 3.88446(2) Å c = 3.88351(5) Å
lattice parameters of orthorhombic phase	a = 5.33435(2) A b = 5.38713(1) A c = 7.58684(2) A	a = 5.33066(3) Å b = 5.38543(3) Å c = 7.58256(6) Å		

Table 2. Rietveld Refinement Results for $Na_{1-x}K_xOsO_3 \ \ x = 0.65$ and 0.75) as Measured by SXRD at Room Temperature

_		
x	0.65	0.75
space group	P4/mmm	P4/mmm
a (A)	3.88235(2)	3.88446(2)
c (A)	3.88016(4)	3.88351(5)
V (Å ³)	58.4844(7)	58.5985(9)
occupancy of potassium at A-site	0.573	0.77
$d_{\rm cal}~({\rm g/cm^3})$	7.679	7.754
U_{ij} of A-site (10 ⁻³ Å ²)	$U_{11} = 2.5(7)$	$U_{11} = 9(1)$
	$U_{33} = 13(2)$	$U_{33} = 10(2)$
U_{ij} or U_{iso} of Os site (10^{-3} Å^2)	$U_{\text{iso}} = 3.77(4)$	$U_{11} = 7.6(3)$
		$U_{33} = 3(4)$
U_{iso} of oxygen site (10^{-3} Å^2)	$U_{\text{iso}}(O1) = 6(4)$	$U_{\text{iso}}(O1) = 10(6)$
	$U_{\text{iso}}(O2) = 6(2)$	$U_{\text{iso}}(O2) = 8(3)$
final R values (\boxtimes)	$R_{wp} = 8.004$	$R_{wp} = 7.521$
	$R_p = 5.789$	$R_{\rm p} = 5.607$
	$R_{\rm B} = 3.225$	$R_{\rm B} = 1.898$
	$R_{\rm F}=1.292$	$R_{\rm F} = 1.184$

^aGeneral atomic positions for P4/mmm (no. 123): A 1a (0, 0, 0), Os 1d (0.5, 0.5, 0.5), O1 1c (0.5, 0.5, 0), and O2 2e (0.5, 0, 0.5). Anisotropic displacement parameters $(U_{ij}, 10^{-3} \text{ Å}^2)$ for 1a and 1d: $U_{11} = U_{22}$, $U_{12} = U_{13} = U_{23} = 0$. The isotropic displacement parameter is represented by U_{iso} .

Table 3. Rietveld Refinement Results for $Na_{1-x}K_xOsO_3 \boxtimes x = 0.65$ and 0.75) as Measured by SXRD at 100 K^{\boxtimes}

x	0.65	0.75
space group	$R\overline{3}m$	$R\overline{3}m$
a (A)	5.48901(2)	5.49213(2)
c (A)	6.71015(3)	6.71427(2)
V (Å3)	175.086(1)	175.393(1)
occupancy of potassium at A-site	0.573(6)	0.77(1)
d_{cal} (g/cm ³)	7.695	7.770
U _{ij} of A-site (10 ⁻³ Å ²)	$U_{11} = 0.8(3)$	$U_{11} = 4.2(3)$
	$U_{33} = 3.8(6)$	$U_{33} = 8.3(6)$
U_{ij} of Os site (10^{-3} Å^2)	$U_{11} = 2.57$ (6)	$U_{11} = 3.54(7)$
	$U_{33} = 2.4(1)$	$U_{33} = 4.0(1)$
$U_{\rm iso}$ of oxygen site (10^{-3} Å^2)	3.8(3)	6.0(3)
final R values (□)	$R_{wp} = 7.192$	$R_{wp} = 7.244$
	$R_p = 5.022$	$R_p = 5.389$
	$R_{\rm B} = 3.411$	$R_{\rm B} = 1.747$
	$R_{\rm F} = 1.088$	$R_{\rm F} = 0.960$

^aGeneral atomic positions for $R\overline{3}m$ (no. 166): A 3b (0, 0, 0.5), Os 3a (0, 0, 0), and O 9d (0.5, 0, 0.5). Anisotropic displacement parameters (U_{ij} 10^{-3} Å²) for 3b and 3a: $U_{11} = U_{22} = 2 \times U_{12}$, $U_{13} = U_{23} = 0$. Isotropic displacement parameter is represented by U_{iso} .

Figure 4 shows the evolution of the crystal structures and their lattice parameters as a function of temperature. The same structural consequence at low temperatures is found in $Na_{1-x}K_xOsO_3$ (x > 0.6). The Na-substitution in these perovskites lowers the R-T and T-C phase transitions by ~20 K from those for KOsO₃. It should be noted that the R-T and T-C phase transitions in $Na_{1-x}K_xOsO_3$ (x = 0.75) show a slight increase compared to $Na_{1-x}K_xOsO_3$ (x = 0.65), as indicated by the DSC measurements, as shown in Figure 5. From the DSC curves, it is observed that the temperatures of the R-T and T-C transitions in sample x = 0.65 are 220 and 308 K, respectively, while in sample x = 0.75, they are 222 and

Table 4. Rietveld Refinement Results for $Na_{1-x}K_xOsO_3 \boxtimes x = 0.65$ and 0.75) as Measured by SXRD at 400 K^{\boxtimes}

x	0.65	0.75
space group	$Pm\overline{3}m$	$Pm\overline{3}m$
a (Å)	3.88426(1)	3.88661(1)
V (Å ³)	58.6038(2)	58.7101(2)
occupancy of potassium at A-site	0.573	0.77
d_{cal} (g/cm ³)	7.663	7.739
U_{ij} of A-site (10^{-3} Å^2)	$U_{11} = 7.6(3)$	$U_{11} = 11.7(2)$
U_{ij} of Os site (10^{-3} Å^2)	$U_{11} = 4.60(4)$	$U_{11} = 5.92(5)$
U_{ii} of oxygen site (10^{-3} Å^2)	$U_{11} = 7(1)$	$U_{11} = 3(1)$
	$U_{22} = 8.0(8)$	$U_{22} = 15.2(9)$
Final R values (2)	$R_{wp} = 8.722$	$R_{wp} = 8.208$
	$R_{\rm p} = 6.196$	$R_{\rm p} = 6.245$
	$R_{\rm B} = 3.558$	$R_{\rm B} = 1.947$
	$R_{\rm F} = 1.433$	$R_{\rm F} = 1.147$

^aGeneral atomic positions for Pm-3m (no. 221): A 1a (0, 0, 0), Os 1b (0.5, 0.5, 0.5), and O 3c (0, 0.5, 0.5). Anisotropic displacement parameters $(U_{ij}, 10^{-3} \text{ A}^2)$ for 1a and 1b: $U_{11} = U_{22} = U_{33}, U_{12} = U_{13} = U_{23} = 0$. For 3c, the parameters are $U_{22} = U_{33}, U_{12} = U_{13} = U_{23} = 0$.

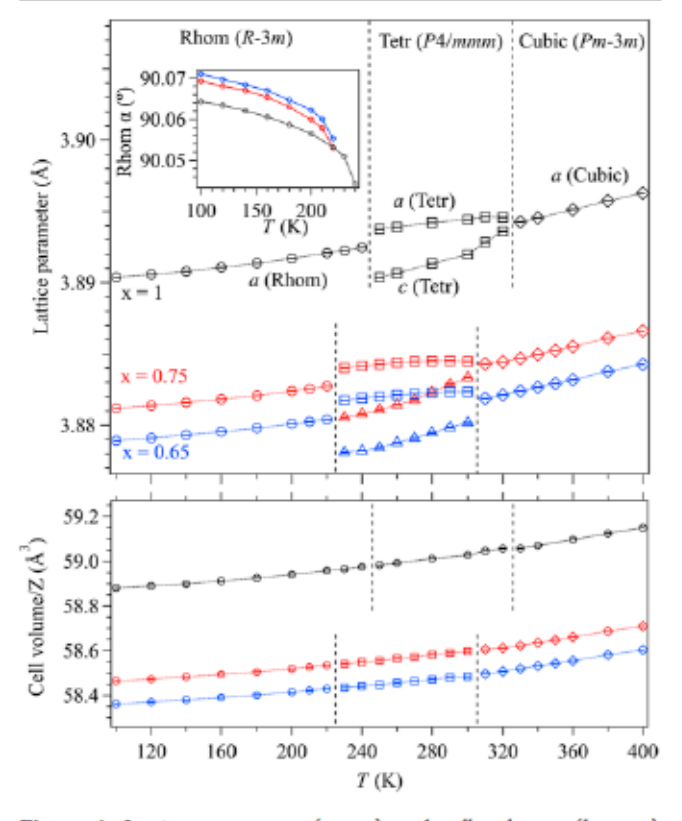


Figure 4. Lattice parameters (upper) and cell volumes (bottom) versus temperature for $Na_{1-x}K_xOsO_3$ (x = 0.65, 0.75, and 1). The angles of rhombohedral phase versus temperature are shown in the inset.

312 K. This small difference is not discernible in SXRD measurement because of a larger temperature interval between sampling points. The structural distortion in the R phase reflects in a slight deviation from 90° in the unit cell. The temperature dependence of the rhombohedral is shown in the inset of Figure 4.

3.2. Physical Properties. All the samples of $Na_{1-x}K_xOsO_3$ synthesized under 14 GPa come as powder with grain size in the range 20–500 μ m after opening the Pt crucible. The

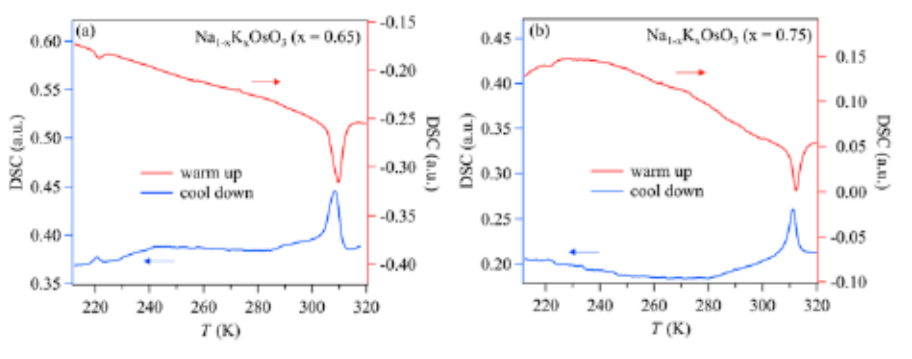


Figure 5. Results of differential scanning calorimetry of $Na_{1-x}K_xOsO_3$ (a) x = 0.65 and (b) x = 0.75.

standard four-probe and Hall bar patterns were created on the surface of rectangular crystals fabricated by the focused ion beam (FIB). Unfortunately, the surface quality is deteriorated severely after FIB; results of the resistivity measurement no longer reflect the bulk property. Instead, we measured the temperature dependence of thermoelectric power S(T) of the cold-pressed samples of $\mathrm{Na_{1-x}K_xOsO_3}$ for monitoring the evolution of electronic state in these phases as a function of x and temperature.

In the insulator phase of parent compound NaOsO₃, the gap opening at the Fermi energy does not lead to the typical behavior for a semiconductor or an insulator. Instead, S(T) in Figure 6 manifests a broad hump in the magnitude near 200 K.

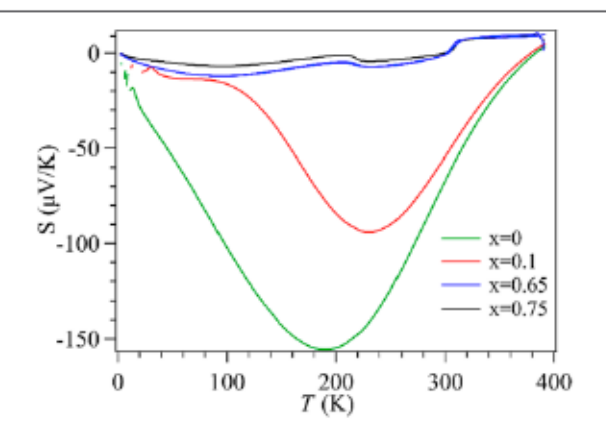


Figure 6. Temperature dependences of the thermoelectric power (S) of $Na_{1-x}K_xOsO_3$ (x = 0, 0.1, 0.65, and 0.75).

Without a sound model to fit the S(T) in the insulator phase, we use it as the benchmark for the insulator phase in the study of electronic state evolution in the Na_{1-x}K_xOsO₃ series. Although there is no reliable indication of the K-substitution in the sample of x = 0.10 from the structural study, the Ksubstitution reduces the maximum value of |S(T)| near 200 K. In the two-phase coexistence, the thermoelectric power is weighted by conductivity σ of individual components as S = $(\sigma_1S_1 + \sigma_2S_2)/(\sigma_1 + \sigma_2)$. The magnitude reduction of S(T) in the x = 0.10 sample is more likely dominated by the contribution from a small and temperature-independent S(T)in a more conducting tetragonal phase from the structural study. A similar situation also happens in the x = 0.6 sample, where an even larger phase volume of the tetragonal phase is found. As a result, S(T) in this sample is dominated by that seen in the single-phase samples of x = 0.65 and 0.75. The S(T) for the x = 0.65 sample is typical for the tetragonal phase $Na_{1-x}K_xOsO_3$. The magnitude of S(T) in this sample is small,

consisting of a metallic phase. More importantly, there are clear anomalies at the phase transitions from the R to T and T to C phase.

The magnetic susceptibility $\chi(T)$ of the x=0.65 and 0.75 samples are featureless, as shown in Figure 7. The kink around 50 K is due to the contribution from a minor infiltration of oxygen into the sample space in the MPMS. However, the nonlinear M-H curves of the x=0.65 and 0.75 samples indicate a weak ferromagnetism in a magnetic ordered phase with the Curie temperature T_c above room temperature. There are still tiny impurity phases such as Os metal and OsO₂ in the samples. As confirmed in separate measurements, these materials are not magnetic to 4 K.

4. DISCUSSION

The geometric tolerance factor $t = (A-O)/(B-O)\sqrt{2}$ reflects the bond length mismatch in the perovskite structure. A cubic perovskite is always found for t values close to 1. The octahedral site tilting systems are developed to accommodate the bond length mismatch created in perovskites with t < 1. There are 15 tilting systems which can be organized through groups and their subgroups based on their structural symmetries. 12,13 Depending on the charge configurations, i.e., $A^{1+}B^{5+}O_3$, $A^{2+}B^{4+}O_3$, and $A^{3+}B^{3+}O_3$, varying t factor through either the chemical substitution and changing temperature leads to the structural distortions through a particular pathway in the tilting systems. It should be noted that all the ferroelectric phases with breaking the inversion symmetry in perovskite $BaTiO_3$ with t > 1 are not within the 15 tilting systems.

There are examples of perovskite systems exhibiting the complete structural evolution between orthorhombic and cubic perovskite phases as t = 1 is approached from t < 1. For instance, Ca_{1-x}Sr_xFeO_y 14 Sr_{1-x}Ba_xRuO_y 15 and (Ca, Sr, and Ba)OsO₃¹⁶ represent 3d-, 4d-, and 5d- perovskite oxides, respectively. Through larger atom substitution in the A-site, all of the series undergo a subsequent phase transition from orthorhombic to cubic perovskite structure. The cubic perovskite structure (Pm3m) is observed in $Ca_{1-x}Sr_xFeO_3$ (x≥ 0.8), whereas the structure of Sr_{1-x}Ba_xRuO₃ changes from the Pbnm phase to the Pm3m phase ($x \ge 0.4$) with an intermediate phase, Imma phase (x = 0.2-0.3). It is common in the A2+B4+O3 perovskites that the tilting system changes from $a^0a^0a^0$ of the $Pm\overline{3}m$ phase to $a^-a^-c^+$ of the Pbnm phase with intermediate phases $a^0b^-b^-$ of the Imma phase and $a^0a^0c^$ of the I4/mcm phases between them. 17 The success in highpressure synthesis of KOsO3 perovskite has enabled the demonstration of the complete evolution from the orthorhombic perovskite NaOsO3 to the cubic phase of the

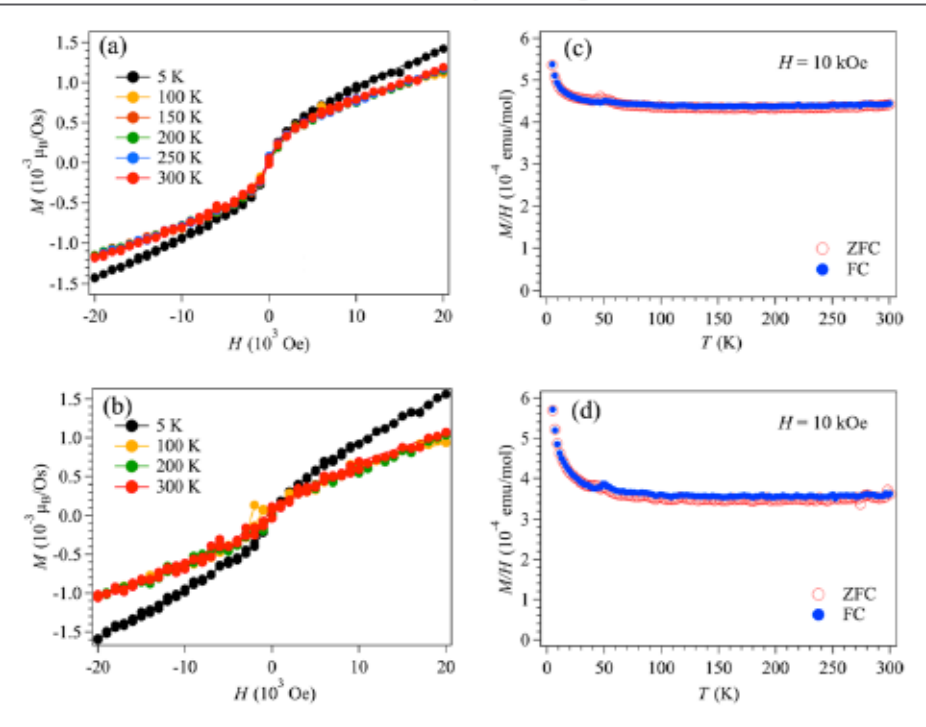


Figure 7. Field dependences of the magnetization of $Na_{1-x}K_xOsO_3$: (a) x = 0.65 and (b) x = 0.75; temperature dependences of the magnetization of (c) x = 0.65 and (d) x = 0.75.

perovskite KOsO₃ at T > 320 K. Unfortunately, a complete solid-state solution can only be found in the cubic phase with x > 0.6 in Na_{1-x}K_xOsO₃. The presence of Na ions in the tetragonal phase for $x \ge 0.6$ in $Na_{1-x}K_xOsO_3$ reduces the lattice parameters slightly. A noticeable jump in the lattice marameters from x = 0.65 to 0.6 in Figure 1 indicates that the Na concentration in the tetragonal phase within the two phase region decreases. On the Na end of the series, it appears that a negligible concentration of K can be accommodated in the orthorhombic structure. It is intereasting to study the series of $Ca_{1-x}Ba_xOsO_3$ to find out whether lacking the solid solution in the orthorhombic perovskite is peculiar for NaOsO3. The twophase coexistence is found in the substitution range $0 < x \le$ 0.6. The lattice parameters in these two phases are nearly independent to x, which implies that there is a negligible K doping in the orthorhombic phase and the maximum Na concentration in the tetragonal phase is about 0.4.

The calculation based on bond lengths from experiments shown in Figure 8 gives a t = 1.000 at room temperature and 0.9999 at 100 K for x = 0.65 and 0.75 in $Na_{1-x}K_xOsO_3$. On the other hand, the calculation based on tabulated ionic size via SPuDs¹⁸ gives a t = 1.0423 and a t = 1.072 for x = 0.5 and 0.75, respectively. Therefore, the (Na, K)-O bonds in the perovskite structure must be under compression, whereas the Os-O bonds are under tension in the products of highpressure synthesis. It is understandable that the average (Na, K)—O bond length reduces as x decreases because of the reduction of the mean ionic size at the A-site of the perovskite structure, which also releases somehow the tension stress on the Os-O bonds. The variation of the tension stress on the Os-O bond as a function of x in the cubic phase is also reflected in the bond valence sum (BVS). There is no Os(5) in SpuDs software. 18 The BVS for Os in Na_{1-x}K_xOsO₃, shown in Figure 8, are calculated by BVS = $\sum_{i=1}^{N} v_i$ where $v_i = e^{(R_0 - i)^3/B}$, N is the coordination number, l is the bond length, B = 0.37, ¹⁹ and $R_0(Os^{5+}) = 1.867$. A BVS of 4.83 indicates that Os-O in

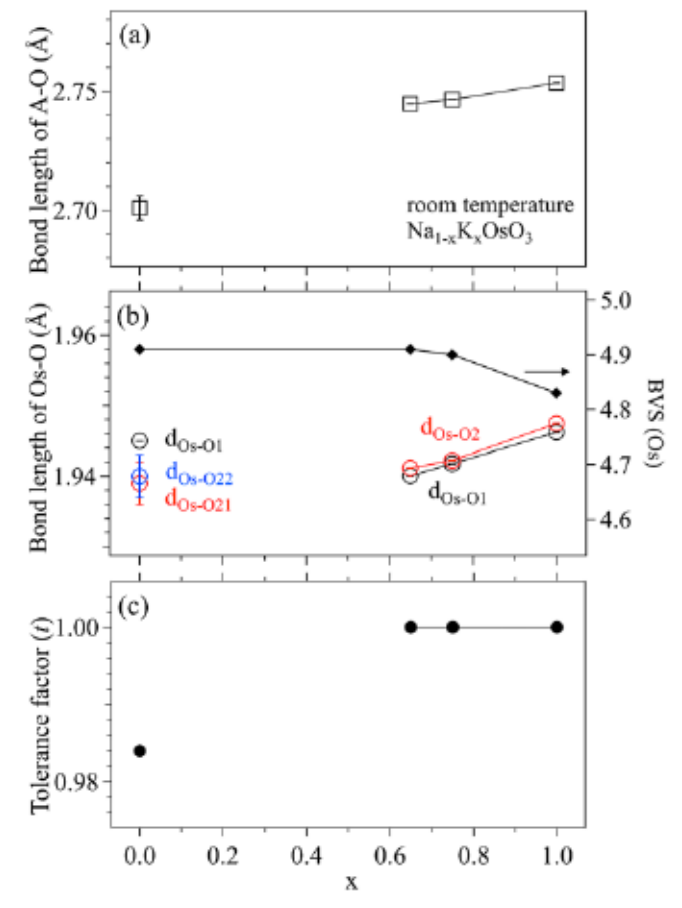


Figure 8. Room-temperature bond length of (a) A–O, (b) Os–O, and BVS for Os and (c) calculated tolerance factor (t) for $Na_{1-x}K_xOsO_3$ (x=0,0.65,0.75, and 1).

 $KOsO_3$ is underbonding due to the tension stress. It is gradually improved to BVS = 4.91 for the x = 0.65 sample. The

Table 5. Comparison of the Room-Temperature Structural Parameters of Na_{1-x}K_xOsO₃ Perovskite Oxides[™]

0 6 GPa Pbnm 5.32817(1) 5.38420(1)
Pbnm 5.32817(1)
5.32817(1)
5.38420(1)
7.58038(1)
54.3664(3)
2.492(5)VIII; 2.701(5)XI
$1.945(1) \times 2$
$1.940(3) \times 2$
$1.939(3) \times 2$
1.941(2)
9.7516
0.908 ^{VIII} ; 0.984 ^{XII}
153.9(3)
155.2(2)
154.6(3)

^aTolerance factors are calculated by $t = \langle A-O \rangle/\langle B-O \rangle/\sqrt{-}$, where $\langle A-O \rangle$ and $\langle B-O \rangle$ represent the average bond lengths obtained from structure refinement. The structural parameters of NaOsO₃ are used from ref 3.

underbonding M-O can also be found in all perovskites with a 180° M-O-M bond angle, which are synthesized under high pressure, for instance, BVS = 3.85 in $BaIrO_3$, ²¹ 3.77 in $BaRuO_3$, ²² and 3.477 in $BaOsO_3$, ¹⁶ An entire evolution from the overbonding to underbonding can be found in $Ca_{1-x}Sr_xMnO_3$ and $Sr_{1-y}Ba_yMnO_3$, BVS = 4.14 for $Ca_{0.8}Sr_{0.2}$ 4.04 for Ca_{0.9}Sr_{0.1}, 4.0056 for Sr, 3.935 for Sr_{0.9}Ba_{0.1}, and 3.867 for Sr_{0.8}Ba_{0.2}. ²³ The two-step synthesis route appears to play a significant role in making the Mn-O bonds under tension stress in these manganites. In contrast, the compressive stress on the M-O array in the orthorhombic RMO_3 is released by the octahedral site rotations. In these cases, a BVS, which is extremely close to their formal valence value, is obtained, for example, BVS = 3.0 ± 0.09 in RFeO₃ and 3.0 ± 0.04 in RCrO₃. All the M-O bond lengths used are from ref 24. It remains puzzling to understand the underbonding of Os-O in orthorhombic NaOsO₂

In the perovskite ABO3, the competition for the bonding covalency with oxygen 2p between the A-O and B-O bonds is correlated with the charge configuration. The structural evolution found in ATaO3 perovskites provides a good template for us to study the structures in AOsO3, where A = alkaline. At room temperature, KTaO3 crystallizes into a cubic perovskite structure, 25 whereas NaTaO3 has been identified as exhibiting phase coexistence of two orthorhombic structures with Pbnm and Cmcm (a0b+c-) space groups.26 The $Na_{1-x}K_xTaO_3$ samples maintain the cubic structure until x =0.28, with the tetragonal structure P4/mmm appearing when x= 0.16.27 The author pointed out in the paper that crystal growth encountered difficulties when attempting to grow $Na_{1-x}K_xTaO_3$ crystal samples with 0.16 < x < 0.26. This challenge may be attributed to a miscibility gap existing within the range between the cubic and tetragonal phases, potentially impeding crystal growth. An almost linear relationship between the lattice parameter of $Na_{1-x}K_xTaO_3$ (x > 0.28) and x is observed, similar to what can be seen in $Na_{1-x}K_xOsO_3$ (x = 0.65, 0.75, and 1). The lattice parameter undergoes a significant decrease from the cubic phase to the orthorhombic phase in Na1-xKxTaO3, resembling the behavior observed in the case of Na1-xKxOsO3. In a structural study as a function of temperature, Darlington and Knight have shown the change of

the tilting system from $a^0a^0a^0$ ($Pm\overline{3}m$) to $a^0b^0c^+$ (P4/mbm), to $a^0b^-c^+$ (Cmcm), to $a^-a^-c^+$ (Pbnm) as temperature decreases from 1050 to 750 K in NaNbO₃ and NaTaO₃. Lacking the solid solution for x < 0.65 in Na_{1-x}K_xOsO₃ prevents us from studying the tilting systems that may develop between the orthorhombic phase and the cubic phase.

The ideal perovskite structure is cubic in space group Pm3m, which belongs to point group Oh. According to the existing perovskite compounds, three possible types of distortion can lead to distorted perovskite structures: octahedral site distortions, displacement of B cation including ferroelectric and antiferroelectric displacements, and octahedral site tilting.29 These distortions are also accompanied by A-site cation dislocation. The majority of distorted perovskites derived from the parent cubic perovskite structure can be obtained through the tilting of the octahedra. Howard and Stokes conducted a thorough group analysis, focusing on octahedral tilting, resulting in 14 subgroups from the cubic perovskite structure. 13 Since the Os-O bonds are under tension stress in $Na_{1-x}K_xOsO_3$ (x > 0.6), any structural distortions can be only made without the octahedral site rotations. As shown in Table 5 and Figure 9, the octahedral

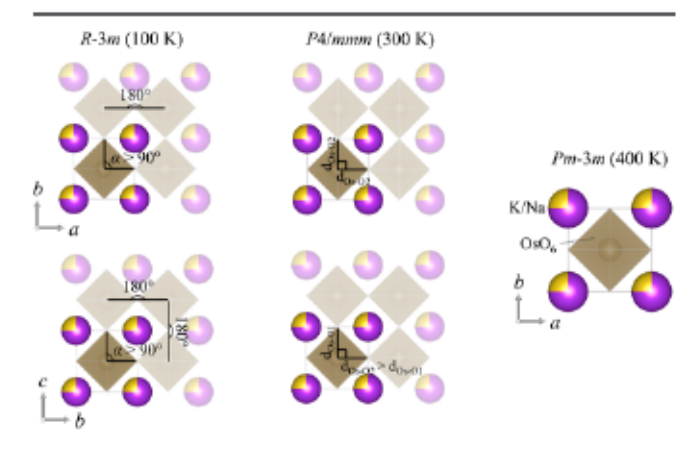


Figure 9. Structure models for $Na_{1-x}K_xOsO_3$ (x = 0.65 and 0.75) at different temperatures. The tetragonal (P4/mmm) and rhombohedral ($R\overline{3}m$) structures contain multiple unit cells.

tilting of Os-O-Os remains at 180° in the three phases throughout the entire temperature range from 100 to 400 K. The T (P4/mmm) and R (R3m) perovskite structures do not belong to the subgroup derived from octahedral tilting. The unit cell volume decreases smoothly through the phase transition from C to T and T to R in perovskites Na_{1-x}K_xOsO₃ $(x \ge 0.65)$ as temperature decreases, as shown in Figure 4. Within the space group Oh1, there are 32 subgroups with unchanged unit cells, encompassing P4/mmm (D_{3d}^{5}) and R3m $(D_{4h}^{-1})^{30}$ Additionally, the coordinates of the A-site and B-site atoms in perovskite $Na_{1-x}K_xOsO_3$ ($x \ge 0.65$) remain unchanged in the distorted phases, with the symmetry alteration attributed solely to the deformation of the unit cell. In the T (P4/mmm) phase, the deformation of the unit cell is reflected in the presence of two shorter Os-O along the c axis and four longer Os-O in the ab plane. In the R (R3m) phase, it results in O-Os-O angles deviating slightly from

A sharp difference between the d⁰ A¹⁺B⁵⁺O₃ perovskites and $Na_{1-x}K_xOsO_3$ ($x \ge 0.65$) in terms of subgroup structures deviating from the cubic phase as temperature decreases makes it unlikely that the elastic energy originates the phase transitions in the latter. With the t2g eg configuration in Na1-xKxOsO3, orbital angular momentum L is quenched in the L-S coupling. However, the spin-orbit coupling (SOC) is to play an important role in the j-j coupling in these 5d perovskites. In NaOsO3, the anomaly of lattice parameters on crossing the metal-insulator transition can be well simulated only if the SOC is considered.6 The subtle local structural distortions in the T and R phase in $Na_{1-x}K_xOsO_3$ (x > 0.6) may manifest the higher order instabilities of the electronic structure. The transition temperatures of T to C phase shifts to lower temperature by ~ 20 K from the perovskite x = 1 to x = 10.75 and 0.65. In perovskite RAIO3 where the phase transitions are triggered for purely the lattice elastic energy in origin, however, the transition temperature increases for the phase transition from a lower symmetry phase to the cubic phase as t factor decreases.31 This observation aligns with the hypothesis that the phase transitions in $Na_{1-x}K_xOsO_3$ ($x \ge 0.65$) have an electronic origin.

5. CONCLUSIONS

The osmate perovskites $Na_{1-x}K_xOsO_3$ (x > 0.1) was synthesized for the first time under high-pressure and hightemperature conditions. The solid-solution of Na_{1-x}K_xOsO₃ in the tetragonal phase at room temperature can only be found for $x \ge 0.65$. The two-phase coexistence (Pbnm and P4/mmm) is found in the samples with 0 < x < 0.65. The structural determination of the samples of $Na_{1-x}K_xOsO_3$ with $x \ge 0.65$ over 100-400 K reveals the phase transitions from the cubic phase (Pm3m) to the tetragonal phase (P4/mmm) at ~ 320 K and subsequently to the rhombohedral phase (R3m) at ~ 230 K. The phase diagram of osmate perovskite Na_{1-x}K_xOsO₃ is shown in Figure 10. In sharp contrast to the tilting systems developed due to the bond length mismatch in the do A1+B5+O3 perovskites, the distortions in the low-symmetry P4/mmm and R3m phases are characterized by a slight change of local bond lengths and a slight deviation of the unit cell angle from 90°. These distorted structures in the perovskite $Na_{1-x}K_xOsO_3$ ($x \ge 0.65$) do not belong to the tilting systems in perovskites reported. The structural comparison between the phases found in $Na_{1-x}K_xOsO_3$ with $x \ge 0.65$ and those in the do A1+B5+O3 perovskites and the structural analysis based

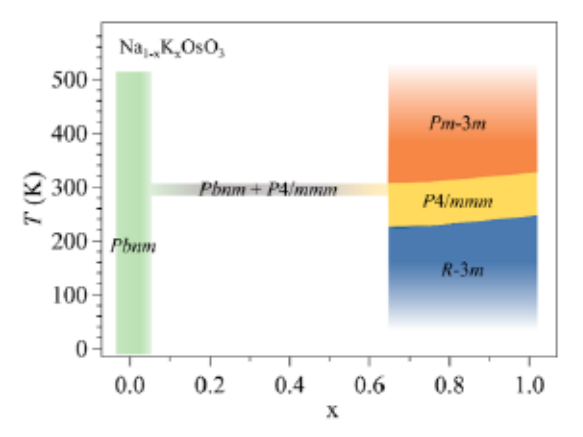


Figure 10. Phase diagram of Na_{1-x}K_xOsO₃.

on BVS imply that the driving force for the phase transitions is likely from the electron structural instability. The perovskites $Na_{1-x}K_xOsO_3$ ($x \ge 0.6$) appear to be metallic at least up to 400 K in the cubic, tetragonal, and rhombohedral phases and magnetic at least up to 300 K.

AUTHOR INFORMATION

Corresponding Author

Jianshi Zhou — Materials Science and Engineering Program, Department of Mechanical Engineering, University of Texas at Austin, Austin, Texas 78712, United States; ⊚ orcid.org/ 0000-0002-7667-5640; Email: jszhou@mail.utexas.edu

Authors

Jie Chen – Materials Science and Engineering Program, Department of Mechanical Engineering, University of Texas at Austin, Austin, Texas 78712, United States; orcid.org/ 0000-0001-9609-669X

Alexei A. Belik — Research Center for Materials Nanoarchitectonics MANA), National Institute for Materials Science, Tsukuba, Ibaraki 305-0044, Japan; ⊙ orcid.org/0000-0001-9031-2355

Kazunari Yamaura — Research Center for Materials
Nanoarchitectonics MANA), National Institute for
Materials Science, Tsukuba, Ibaraki 305-0044, Japan;
Graduate School of Chemical Sciences and Engineering,
Hokkaido University, Sapporo, Hokkaido 060-0810, Japan;
orcid.org/0000-0003-0390-8244

Complete contact information is available at: https://pubs.acs.org/10.1021/acs.chemmater.4c00568

Notes

The authors declare no competing financial interest.

ACKNOWLEDGMENTS

This research was primarily supported by the National Science Foundation through the Center for Dynamics and Control of Materials: an NSF MRSEC under Cooperative Agreement no. DMR-2308817. This work was partially supported by a Grantin-Aid for Scientific Research (no. JP22H04601) from the Japan Society for the Promotion of Science and the Kazuchika Okura Memorial Foundation (no. 2022-11). Synchrotron radiation was used at the powder diffraction beamline BL02B2 at SPring-8, with permission from the Japan Synchrotron Radiation Research Institute (Proposal Numbers: 2023A1496, 2023A2361, and 2023B1676). MANA is

supported by the World Premier International Research Center Initiative (WPI), MEXT, Japan.

REFERENCES

- (1) Shi, Y.; Guo, Y.; Wang, X.; Princep, A. J.; Khalyavin, D.; Manuel, P.; Michiue, Y.; Sato, A.; Tsuda, K.; Yu, S.; Arai, M.; Shirako, Y.; Akaogi, M.; Wang, N.; Yamaura, K.; Boothroyd, A. T. A ferroelectric-like structural transition in a metal. *Nat. Mater.* 2013, 12 (11), 1024–1027.
- (2) Anderson, P. W.; Blount, E. I. Symmetry Considerations on Martensitic Transformations: "Ferroelectric" Metals? Phys. Rev. Lett. 1965, 14 (7), 217-219.
- (3) Shi, Y. G.; Guo, Y. F.; Yu, S.; Arai, M.; Belik, A. A.; Sato, A.; Yamaura, K.; Takayama-Muromachi, E.; Tian, H. F.; Yang, H. X.; Li, J. Q.; Varga, T.; Mitchell, J. F.; Okamoto, S. Continuous metal-insulator transition of the antiferromagnetic perovskite NaOsO₃. Phys. Rev. B 2009, 80 (16), 161104.
- (4) Slater, J. C. Magnetic Effects and the Hartree-Fock Equation. Phys. Rev. 1951, 82 (4), 538-541.
- (5) Vale, J. G.; Calder, S.; Donnerer, C.; Pincini, D.; Shi, Y. G.; Tsujimoto, Y.; Yamaura, K.; Sala, M. M.; van den Brink, J.; Christianson, A. D.; McMorrow, D. F. Evolution of the Magnetic Excitations in NaOsO₃ through its Metal-Insulator Transition. *Phys. Rev. Lett.* 2018, 120 (22), 227203.
- (6) Zhou, J. S.; Li, X. Y.; Johannes, M. D. Evidence of electronic structural change at the metal-insulator transition in the perovskite NaOsO₃. Phys. Rev. B 2023, 108 (19), 195115.
- (7) Chen, J.; He, J.; Zhang, Y.; Chariton, S.; Prakapenka, V.; Yamaura, K.; Lin, J.-F.; Goodenough, J. B.; Zhou, J. S. In situ structural determination of 3d and 5d perovskite oxides under high pressure by synchrotron x-ray diffraction. Phys. Rev. B 2023, 108 (13), 134106.
- (8) Chen, J.; Li, H.; Gainza, J.; Munoz, A.; Alonso, J. A.; Liu, J.; Chen, Y.-S.; Belik, A. A.; Yamaura, K.; He, J.; Li, X.; Goodenough, J. B.; Zhou, J. S. Exotic Magnetism in Perovskite KOsO3. *Phys. Rev. Lett.* 2024, 132 (15), 156701.
- (9) Izumi, F.; Momma, K. Three-Dimensional Visualization in Powder Diffraction. Solid State Phenom. 2007, 130, 15–20.
- (10) Momma, K.; Izumi, F. VESTA 3 for three-dimensional visualization of crystal, volumetric and morphology data. J. Appl. Crystallogr. 2011, 44 (6), 1272–1276.
- (11) Tsuda, K.; Tanaka, M. Refinement of crystal structure parameters using convergent-beam electron diffraction: the lowtemperature phase of SrTiO₃. Acta Crystallogr., Sect. A 1995, 51 (1), 7-19.
- (12) Aleksandrov, K. S. The sequences of structural phase transitions in perovskites. Ferroelectrics 1976, 14 (1), 801–805.
- (13) Howard, C. J.; Stokes, H. T. Group-Theoretical Analysis of Octahedral Tilting in Perovskites. Acta Crystallogr., Sect. B: Struct. Sci., Cryst. Eng. Mater. 1998, 54 (6), 782–789.
- (14) Takeda, T.; Kanno, R.; Kawamoto, Y.; Takano, M.; Kawasaki, S.; Kamiyama, T.; Izumi, F. Metal-semiconductor transition, charge disproportionation, and low-temperature structure of Ca_{1-x}Sr_xFeO₃ synthesized under high-oxygen pressure. Solid State Sci. 2000, 2 (7), 673–687.
- (15) Cheng, J. G.; Zhou, J. S.; Goodenough, J. B. Lattice effects on ferromagnetism in perovskite ruthenates. Proc. Natl. Acad. Sci. U.S.A. 2013, 110 (33), 13312–13315.
- (16) Shi, Y.; Guo, Y.; Shirako, Y.; Yi, W.; Wang, X.; Belik, A. A.; Matsushita, Y.; Feng, H. L.; Tsujimoto, Y.; Arai, M.; Wang, N.; Akaogi, M.; Yamaura, K. High-Pressure Synthesis of 5d Cubic Perovskite BaOsO₃ at 17 GPa: Ferromagnetic Evolution over 3d to 5d Series. J. Am. Chem. Soc. 2013, 135 (44), 16507–16516.
- (17) Howard, C. J.; Knight, K. S.; Kennedy, B. J.; Kisi, E. H. The structural phase transitions in strontium zirconate revisited. J. Phys.: Condens. Matter 2000, 12 (45), L677–L683.
- (18) Lufaso, M. W.; Woodward, P. M. Prediction of the crystal structures of perovskites using the software program SPuDS. Acta

- Crystallogr., Sect. B: Struct. Sci., Cryst. Eng. Mater. 2001, 57 (6), 725–738.
- (19) Brese, N. E.; O'Keeffe, M. Bond-valence parameters for solids. Acta Crystallogr., Sect. B: Struct. Sci., Cryst. Eng. Mater. 1991, 47 (2), 192-197.
- (20) Yamaura, J.-I.; Yonezawa, S.; Muraoka, Y.; Hiroi, Z. Crystal structure of the pyrochlore oxide superconductor KOs₂O₆. J. Solid State Chem. 2006, 179 (1), 336–340.
- (21) Cheng, J. G.; Ishii, T.; Kojitani, H.; Matsubayashi, K.; Matsuo, A.; Li, X.; Shirako, Y.; Zhou, J. S.; Goodenough, J. B.; Jin, C. Q.; Akaogi, M.; Uwatoko, Y. High-pressure synthesis of the BaIrO₃ perovskite: A Pauli paramagnetic metal with a Fermi liquid ground state. *Phys. Rev. B* **2013**, *88* (20), 205114.
- (22) Jin, C.-Q.; Zhou, J.-S.; Goodenough, J. B.; Liu, Q. Q.; Zhao, J. G.; Yang, L. X.; Yu, Y.; Yu, R. C.; Katsura, T.; Shatskiy, A.; Ito, E. High-pressure synthesis of the cubic perovskite BaRuO₃ and evolution of ferromagnetism in ARuO₃ (A = Ca, Sr, Ba) ruthenates. *Proc. Natl. Acad. Sci. U.S.A.* 2008, 105 (20), 7115–7119.
- (23) Chmaissem, O.; Dabrowski, B.; Kolesnik, S.; Mais, J.; Brown, D. E.; Kruk, R.; Prior, P.; Pyles, B.; Jorgensen, J. D. Relationship between structural parameters and the Neel temperature in Sr_{1-x}Ca_xMnO₃ (0<~x<~1) and Sr_{1-y}Ba_yMnO₃ (y<~0.2). Phys. Rev. B 2001, 64 (13), 134412.</p>
- (24) Zhou, J. S.; Alonso, J. A.; Pomjakushin, V.; Goodenough, J. B.; Ren, Y.; Yan, J. Q.; Cheng, J. G. Intrinsic structural distortion and superexchange interaction in the orthorhombic rare-earth perovskites RCrO₃. Phys. Rev. B 2010, 81 (21), 214115.
- (25) Wemple, S. H. Some Transport Properties of Oxygen-Deficient Single-Crystal Potassium Tantalate (KTaO₃). Phys. Rev. 1965, 137 (5A), A1575-A1582.
- (26) Knight, K. S.; Kennedy, B. J. Phase coexistence in NaTaO₃ at room temperature; a high resolution neutron powder diffraction study. Solid State Sci. 2015, 43, 15-21.
- (27) Davis, T. G. Dielectric Properties and Soft Modes in the Ferroelectric Mixed Crystals K_{1-x}Na_xTaO₃. Phys. Rev. B 1972, 5 (7), 2530-2537.
- (28) Darlington, C. N. W.; Knight, K. S. High-temperature phases of NaNbO₃ and NaTaO₃. Acta Crystallogr., Sect. B: Struct. Sci., Cryst. Eng. Mater. 1999, 55 (1), 24–30.
- (29) Howard, C. J.; Stokes, H. T. Structures and phase transitions in perovskites — a group-theoretical approach. Acta Crystallogr., Sect. A 2005, 61 (1), 93—111.
- (30) Goldrich, F. E.; Birman, J. L. Theory of Symmetry Change in Second-Order Phase Transitions in Perovskite Structure. Phys. Rev. 1968, 167 (2), 528-532.
- (31) Mitchell, R. H. Perovskites Modern and Ancient; Almaz Press: Ontario, 2002.